

SAR amplitude probability density function estimation based on a generalized Gaussian scattering model

Gabriele Moser, Josiane Zerubia, Sebastiano B. Serpico

▶ **To cite this version:**

Gabriele Moser, Josiane Zerubia, Sebastiano B. Serpico. SAR amplitude probability density function estimation based on a generalized Gaussian scattering model. RR-5153, INRIA. 2004. inria-00071430

HAL Id: inria-00071430
https://inria.hal.science/inria-00071430

Submitted on 23 May 2006

HAL is a multi-disciplinary open access archive for the deposit and dissemination of scientific research documents, whether they are published or not. The documents may come from teaching and research institutions in France or abroad, or from public or private research centers.

L'archive ouverte pluridisciplinaire **HAL**, est destinée au dépôt et à la diffusion de documents scientifiques de niveau recherche, publiés ou non, émanant des établissements d'enseignement et de recherche français ou étrangers, des laboratoires publics ou privés.

INRIA

INSTITUT NATIONAL DE RECHERCHE EN INFORMATIQUE ET EN AUTOMATIQUE

SAR amplitude probability density function estimation based on a generalized Gaussian scattering model

Gabriele Moser — Josiane Zerubia — Sebastiano B. Serpico

N° 5153

March 2004

THÈME 3



ISSN 0249-6399 ISRN INRIA/RR--5153--FR+ENG

INRIA
SOPHIA ANTIPOLIS

SAR amplitude probability density function estimation based on a generalized Gaussian scattering model

Gabriele Moser* , Josiane Zerubia† , Sebastiano B. Serpico‡

Thème 3 — Interaction homme-machine,
images, données, connaissances
Projet Ariana

Rapport de recherche n° 5153 — March 2004 — 35 pages

Abstract: In the context of remotely sensed data analysis, an important problem is the development of accurate models for the statistics of the pixel intensities. Focusing on Synthetic Aperture Radar (SAR) data, this modelling process turns out to be a crucial task, for instance, for classification or for denoising purposes. In the present report, an innovative parametric estimation methodology for SAR amplitude data is proposed, which takes into account the physical nature of the scattering phenomena generating a SAR image by adopting a generalized Gaussian (GG) model for the backscattering phenomena.

A closed form expression for the corresponding amplitude probability density function (PDF) is derived and a specific parameter estimation algorithm is developed in order to deal with the proposed model. Specifically, the recently proposed "method-of-log-cumulants" (MoLC) is applied, which stems from the adoption of the Mellin transform (instead of the usual Fourier transform) in the computation of characteristic functions, and from the corresponding generalization of the concepts of moment and of cumulant. For the developed GG-based amplitude model, the resulting MoLC estimates turn out to be numerically feasible and are also proved to be consistent.

The proposed parametric approach is validated using several real ERS-1, XSAR, ESAR and airborne SAR images and the experimental results prove that the method models the amplitude probability density function better than several previously proposed parametric models for the backscattering phenomena.

Key-words: Synthetic Aperture Radar (SAR), probability density function, parametric estimation, generalized Gaussian.

* Dept. of Biophysical and Electronic Engineering (DIBE), University of Genoa, Via Opera Pia 11a, I-16145, Genoa (Italy), e-mail: gemini@dibe.unige.it.

† Projet Ariana, UR INRIA Sophia Antipolis, 2004, Route des Lucioles, B.P.93, FR-06902, Sophia Antipolis Cedex (France), e-mail: Josiane.Zerubia@sophia.inria.fr.

‡ Dept. of Biophysical and Electronic Engineering (DIBE), University of Genoa, Via Opera Pia 11a, I-16145, Genoa (Italy), e-mail: vulcano@dibe.unige.it.

Unité de recherche INRIA Sophia Antipolis
2004, route des Lucioles, BP 93, 06902 Sophia Antipolis Cedex (France)
Téléphone : +33 4 92 38 77 77 —Télécopie : +33 4 92 38 77 65

Estimation de la densité de probabilité de l'amplitude d'une image radar de type RSO fondée sur un modèle de diffusion à base de gaussiennes généralisées

Résumé : En télédetection, un problème important est celui de développer des modèles précis pour representer les statistiques des intensités des pixels. En ce qui concerne les données du type Radar à Synthèse d'Ouverture (RSO), cette modélisation constitue un point capital pour la classification ou le débruitage d'une image, par exemple. Dans ce rapport de recherche, une nouvelle méthode d'estimation paramétrique pour les amplitudes d'images RSO est proposée. Elle tient compte de la nature physique des phénomènes de diffusion qui génèrent une image RSO en adoptant une modèle de gaussiennes generalisées pour les phénomènes de rétrodiffusion.

Une expression, sous forme explicite, de la densité de probabilité de l'amplitude est obtenue et un algorithme spécifique d'estimation des paramètres est proposé afin de pouvoir utiliser le modèle proposé. Une mèthode récente fondée sur les "logs-cumulants" est appliquée, dérivant de l'utilisation d'une transformée de Mellin (à la place de la transformée de Fourier usuelle) dans le calcul des fonctions caractéristiques et de la généralisation des concepts de moment et de cumulant correspondante. Les estimées obtenues par la mèthode des log-cumulants pour le modèle d'amplitude fondé sur des gaussiennes généralisées se révelent être calculables numériquement et également consistantes.

Dans ce rapport de recherche, l'approche paramètrique proposée est validée sur diverses images radar RSO (ERS, XSAR, ESAR et des radar aéroportés). Les résultats expérimentaux montrent que la mèthode proposée modèlise mieux la densité de probabilité de l'amplitude que beaucoup de modèles paramétriques proposés précédemment pour les phénomènes de rétrodiffusion.

Mots-clés : Radar à Synthèse d'Ouverture (RSO), densité de probabilité, gaussiennes généralisées.

Contents

1 Introduction **4**

2 A generalized Gaussian model for SAR backscattered signals **7**

3 Estimation of the parameters of the proposed model **9**
3.1 Parameter estimation with the Mellin transform and MoLC 9
3.2 MoLC parametric estimation for the GGR model 11
3.3 Consistency of the proposed estimator 13

4 Experimental results **15**
4.1 Data sets for experiments 15
4.2 PDF estimation results 16

5 Conclusions **20**

Acknowledgments **23**

Appendix **24**
A SAR images employed for experiments 24
B Plots of the estimated PDFs 28

References **33**

1 Introduction

In the context of remotely sensed data analysis, a crucial problem is represented by the need to develop accurate models for the statistics of the pixel intensities. Focusing on Synthetic Aperture Radar (SAR) [5][6][28][33] data, this modelling process turns out to be a crucial task, for instance, for classification [9] or for denoising [28] purposes.

xzFrom a methodological viewpoint, either parametric or non-parametric estimation strategies can be employed for this task [9][10]. Specifically, the parametric approach postulates a given mathematical model for each class-conditional probability density function (PDF) and formulates the PDF estimation problem as a parameter estimation one. Several strategies have been proposed in the literature to deal with parameter estimation, such as the maximum likelihood (ML) methodology [9] or the "method of moments" (MoM) [17][25][40]. On the contrary, non-parametric PDF estimation approaches do not assume any specific analytical model for the unknown PDF, thus providing a larger flexibility, although usually presenting internal architecture parameters to be set by the user [9]. In particular, several non-parametric kernel-based estimation and regression architectures have been proposed in the literature, proving to be effective estimation tools, such as standard Parzen window estimators [9][31], Artificial Neural Networks (ANNs) [1], or Support Vector Machines (SVMs) [22][42][43].

In the present research report, we address the problem of PDF estimation in the specific context of SAR amplitude data analysis. In particular, we focus on parametric estimation strategies, by exploiting an analysis of the physical scattering phenomena generating a SAR image, in order to develop an innovative parametric model, endowed with a consistent estimation strategy. Specifically, the standard model for the statistics of the complex signal backscattered from a given ground area, illuminated by a single-look SAR sensor, adopts a discrete characterization of the phenomena occurring in this area, assuming the number of scatterers to be large and the scatterers to be independent [17][28]. Let us denote as z the complex signal received by the SAR sensor from the ground area $\mathcal{R}$ corresponding to a given pixel, namely:

$$z = x + jy = r\exp(j\theta) = \sqrt{v}\exp(j\theta) \tag{1}$$

where x, y, r, v, θ are the real part, the imaginary part, the amplitude, the intensity, and the phase of the complex signal z, respectively. The standard discrete model for the scattering phenomena assumes the presence in $\mathcal{R}$ of a finite set of n independent scattering entities, thus interpreting z as the result of the interference of the corresponding n contributions. In particular, this interference phenomenon motivates the usual noise-like granular aspect of SAR images, known as speckle [28]. Specifically, assuming the number n of scatterers to be large, according to the central limit theorem [30], the real and the imaginary part of the backscattered signal are assumed to be jointly Gaussian. In particular, they turn out to be independent, zero-mean Gaussian random variables with equal variances, thus yielding an exponential distribution for the signal intensity and a Rayleigh distribution for the signal

amplitude [28], i.e.[1]:

$$p_v(v) = \lambda \exp(-\lambda v), \qquad p_r(r) = 2\lambda r \exp(-\lambda r^2), \quad r, v \geq 0, \tag{2}$$

where λ is a distribution parameter to be estimated according to the image data (for instance, by using ML or MoM [24]). However, real SAR amplitude data often present significantly non-Rayleigh empirical distributions, for instance, exhibiting heavier distribution tails, and thus requiring a more accurate probability density function (PDF) characterization [17][28]. Several different theoretical models for the statistics of the backscattering phenomena have been proposed in order to improve the estimation quality or to generalize the Rayleigh model to different typologies of SAR data. Specifically, the Gamma distribution has been introduced as a model for multi-look SAR intensity PDF, generated by averaging L single-look exponentially distributed intensities, and is expressed as [25][28]:

$$p_v(v) = \frac{(\lambda L)^L}{\Gamma(L)} v^{L-1} \exp(-\lambda L v), \quad v \geq 0, \tag{3}$$

where $\Gamma(\cdot)$ is the standard Gamma function [34]. The corresponding amplitude turns out to be Nakagami-distributed [25][30][40], i.e.:

$$p_r(r) = 2r p_v(r^2) = \frac{2(\lambda L)^L}{\Gamma(L)} r^{2L-1} \exp(-\lambda L r^2), \quad r \geq 0. \tag{4}$$

The Nakagami-Gamma model has also been extended to the case of multilook polarimetric and interferometric data [14][15][19], to finite mixtures of Gamma components [25][27], and its application has been generalized by letting the integer number L of looks be a real positive parameter (interpreted as an "equivalent number of looks", ENL) to be estimated together with λ according to the image data. Both ML and MoM estimates turn out to be feasible for this estimation task [25][40].

In [17] a generalized version of the central limit theorem [20] is applied in order to generalize the standard scattering model by allowing the real and the imaginary part of the backscattered signal to be jointly symmetric-α-stable (SαS) [16][18][20] random variables, thus resulting in the following generalized "heavy-tailed" Rayleigh model for the amplitude PDF:

$$p_r(r) = r \int_0^{+\infty} \rho \exp(-\gamma \rho^\alpha) J_0(r\rho) d\rho, \quad r \geq 0, \tag{5}$$

where α and γ are positive parameters and $J_0(\cdot)$ is the zeroth order Bessel function of the first kind [3][38]. An MoM estimation strategy is developed in [17] for this parametric model.

A different approach to SAR scattering modelling is proposed in [12], by assuming the number n of scatterers to be itself a random variable and the population of scatterers to be

[1] Since the random variables r and v are always non-negative their PDFs are zero on $(-\infty, 0)$. Therefore, hereinafter, we will explicitly define their PDFs only in $[0, +\infty)$.

controlled by a birth-death-migration process. In this case, a K distribution is obtained for the signal intensity [12][13][28], i.e.:

$$p_v(v) = \frac{2(\lambda LM)^{(L+M)/2}}{\Gamma(L)\Gamma(M)} v^{(L+M-2)/2} K_{M-L}\left[2(\lambda LMv)^{1/2}\right], \quad v \geq 0, \tag{6}$$

where λ, L, and M are positive distribution parameters and $K_\nu(\cdot)$ ($\nu > 0$) is the ν-th order modified Bessel function of the second kind [3][38]. The corresponding amplitude distribution is given by:

$$p_r(r) = \frac{4(\lambda LM)^{(L+M)/2}}{\Gamma(L)\Gamma(M)} r^{L+M-1} K_{M-L}\left[2r(\lambda LM)^{1/2}\right], \quad r \geq 0. \tag{7}$$

The same K distribution is obtained when assuming a multiplicative noise model for the SAR intensity, by expressing v as the product of two Gamma distributed components, representing a signal and a noise contribution, respectively [28]. Further extensions of the backscattering modelling approach assuming n as a random variable are proposed in [8][29][44]. MoM turns out to be feasible for the parameter estimation task for a K-distributed random variable [24][28], whereas no close form is available so far for ML parameter estimation, thus requiring intensive numerical computation or analytical approximations of the PDF itself [24][28].

Several generalizations of the MoM estimation strategy have been recently proposed in the specific context of SAR amplitude or intensity parametric estimation, thus focusing on parametric families defined on $[0, +\infty)$. The use of lower, fractional, negative, and complex order moments have been proposed in [26] and in [24] and applied to the fitting of Gamma and K distributions. The corresponding estimates can be proved to exhibit a reduced variance compared to standard MoM estimates [24], although requiring the selection of the optimal order to be employed in the computation of the moments. The same approach has also been applied to the above-mentioned SαS generalized Rayleigh PDF (see Eq. 5) [17]. Furthermore, the recently proposed "method-of-log-cumulants" (MoLC) [24][25][26][40] stems from the adoption of the Mellin transform [38] (instead of the usual Fourier transform) in the computation of characteristic functions [30], and from the corresponding generalization of the concepts of moment and cumulant [30]. The method proves to be feasible for all the above-mentioned parametric models for SAR amplitude and intensity statistics and to provide smaller variance estimates than MoM for Gamma distributed intensities [25]. In the present report, an innovative parametric model is proposed for SAR amplitude data statistics. Specifically, the standard scattering model is generalized by assuming the real and the imaginary part of the backscattered signal to be independent zero-mean generalized Gaussian (GG) [39] random variables and by deriving analytically the resulting amplitude PDF. GGs have been employed for noise modelling in communications, detection, and positioning problems [39], in optical image analysis [2][23], and in wavelet coefficient statistical modelling [21][36][37]. In the present report, the feasibility of such a model for SAR scattering statistical characterization is investigated theoretically and experimentally.

In Section 2 the proposed parametric model is derived and in Section 3 a specific parameter estimation algorithm is developed and proved to be consistent. Section 4 reports the results of the application of the proposed parametric approach to the statistical modelling of the grey-level of several real SAR images, proving the method to better fit the amplitude distribution compared to the previously proposed above-mentioned scattering models. Finally, conclusions are drawn in Section 5.

2 A generalized Gaussian model for SAR backscattered signals

A random variable u is said to be generalized Gaussian if its PDF is given by the following equation [39]:

$$p_u(u) = \frac{\gamma c}{2\Gamma(1/c)} \exp[-|\gamma(u-m)|^c], \quad u \in \mathbb{R}, \tag{8}$$

where $c, \gamma > 0$ and $m \in \mathbb{R}$. Specifically, $m = E\{u\}$ is the expected value of the generalized Gaussian distribution, γ is connected to the variance, thus influencing the dispersion around m, whereas c is a shape parameter, dealing with the sharpness of the PDF. Both the Gaussian distribution and the Laplace one can be viewed as particular cases of this general model, corresponding to $c = 2$ and $c = 1$, respectively.

In this report, we propose to extend the Gaussian model for the real and the imaginary part of the backscattered complex SAR signal z, by assuming them to be distributed according to a generalized Gaussian PDF. Thus, according to the above-mentioned discrete modelling of the scattering phenomena inside the region $\mathcal{R}$, a natural choice is to accept a symmetrical behavior of x and y [28], thus postulating for both random variables the same values of the parameters $\{c, \gamma, m\}$. Similarly, we accept the usual assumptions of independence of these components and of zero mean, thus expressing their joint PDF as follows:

$$p_{xy}(x,y) = p_x(x)p_y(y) = \frac{\gamma^2 c^2}{4\Gamma^2(1/c)} \exp[-\gamma^c(|x|^c + |y|^c)], \quad (x,y) \in \mathbb{R}^2. \tag{9}$$

This choice allows gaining a higher flexibility compared to the standard Gaussian model, by explicitly taking into account the possible non-Gaussian sharpness of the joint PDF p_{xy}, i.e., implicitly allowing the amplitude PDF p_r to exhibit a non-Rayleigh behavior.

Specifically, in order to compute a closed-form expression for p_r, we perform a "rectangular-to-polar" coordinate transformation [30], thus obtaining the following expression for the joint PDF of the signal amplitude $r \geq 0$ and phase $\theta \in [0, 2\pi]$:

$$p_{r\theta}(r,\theta) = r p_{xy}(r\cos\theta, r\sin\theta) = \frac{\gamma^2 c^2 r}{4\Gamma^2(1/c)} \exp[-(\gamma r)^c(|\cos\theta|^c + |\sin\theta|^c)]. \tag{10}$$

Therefore, the corresponding marginal amplitude PDF turns out to be:

$$p_r(r) = \int_0^{2\pi} p_{r\theta}(r,\theta)d\theta = \frac{\gamma^2 c^2 r}{4\Gamma^2(1/c)} \int_0^{2\pi} \exp[-(\gamma r)^c(|\cos\theta|^c + |\sin\theta|^c)]d\theta, \quad r \geq 0. \tag{11}$$

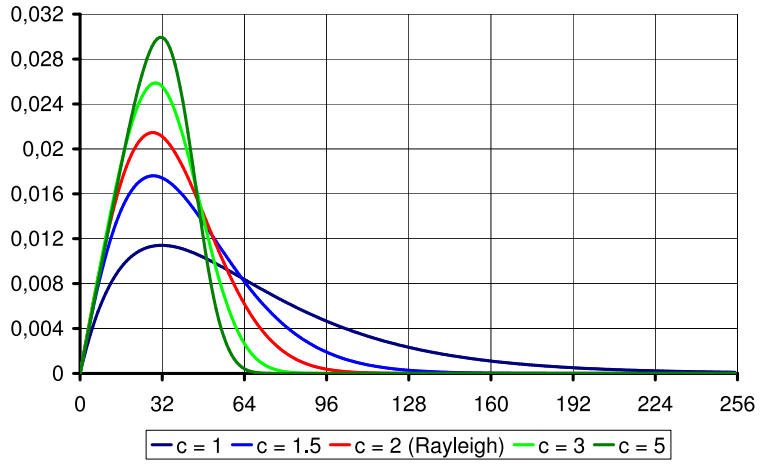


Figure 2.1: Plots of several GGR probability density functions, corresponding to $\gamma = 0.025$ and to several distinct values for c. The value adopted for γ in these examples has been chosen in order to correctly scale the plotted distributions in the range $[0, 255]$ (typical of digital image data).

Since the function $\theta \in [0, 2\pi] \longmapsto |\cos\theta|^c + |\sin\theta|^c$ is $(\pi/2)$-periodical, we finally obtain:

$$p_r(r) = \frac{\gamma^2 c^2 r}{\Gamma^2(1/c)} \int_0^{\pi/2} \exp[-(\gamma r)^c (|\cos\theta|^c + |\sin\theta|^c)] d\theta, \quad r \geq 0. \tag{12}$$

We will refer to this distribution as the Generalized Gaussian Rayleigh (GGR) distribution, since it extends the usual Rayleigh-distributed amplitude model by using generalized Gaussian PDFs. Of course, the Rayleigh PDF can be viewed as a particular case of the GGR distribution, characterized by $c = 2$, i.e.:

$$p_r(r) = \frac{4\gamma^2 r}{\Gamma^2(1/2)} \exp[-(\gamma r)^2] \frac{\pi}{2} = 2\gamma^2 r \exp[-(\gamma r)^2], \quad r \geq 0, \tag{13}$$

since $\Gamma(1/2) = \sqrt{\pi}$ [34].

Fig. 2.1 compares several GGR PDFs, corresponding to a fixed value of γ and to several distinct values of c, both considering the Rayleigh case (i.e., $c = 2$) and several non-Rayleigh PDFs. As highlighted by Fig. 2.1, the GGR parametric family also allows taking into account the possible "heavy tails" behavior of the amplitude data, corresponding to values of c lower than 2. Also a sharper and more impulsive behavior can be obtained for higher values of c (i.e., $c > 2$).

3 Estimation of the parameters of the proposed model

The proposed GGR model for SAR amplitude data is a two-parameter family of PDFs, thus requiring the definition of a suitable estimation procedure, computing for a given SAR amplitude image $\mathcal{I}$, the values of c and of γ which optimally describe the data distribution. From this estimation viewpoint, we consider $\mathcal{I}$ as a set $\mathcal{I} = \{r_1, r_2, \ldots, r_N\}$ of independent and identically distributed (i.i.d.) samples, drawn from the PDF in Eq. (12). This approach is widely accepted in the context of estimation theory [9][10][41] and operatively corresponds to discard in the estimation process the contextual information associated to the correlation between neighboring pixels in the image, thus exploiting only the greylevel information.

First, we stress that the GGR model (12) renders the use of a standard ML estimation approach infeasible. In fact, the i.i.d. assumption allows obtaining the following espression for the log-likelihood function [41] of the image data $\mathcal{I}$:

$$L_{\mathcal{I}}(c,\gamma) = \sum_{k=1}^{N} \ln p_r(r_k) = 2N \left[\ln\gamma + \ln c - \ln\Gamma\left(\frac{1}{c}\right) \right] +$$

$$+ \sum_{k=1}^{N} \ln r_k + \sum_{k=1}^{N} \ln \int_0^{\pi/2} \exp[-(\gamma r_k)^c (|\cos\theta|^c + |\sin\theta|^c)] d\theta. \qquad (14)$$

The ML estimation approach would require the numerical maximization of the function $L_{\mathcal{I}}(\cdot,\cdot)$, which turns out to be a difficult and time-consuming task, due to the presence of the sum of integral contributions in Eq. (14). A much more feasible estimation strategy results if adopting the methods based on the Mellin transform [25].

3.1 Parameter estimation with the Mellin transform and MoLC

The method of log-cumulants (MoLC) has been recently proposed as a parametric PDF estimation technique feasible for distributions defined on $[0, +\infty)$, and has been explicitly applied in the context of the usual parametric families employed for SAR amplitude and intensity data modelling (e.g.: the Nakagami-Gamma and the K distributions) [24][25][27][40]. MoLC is based on the generalization of the usual moment-based statistics, by employing the Mellin transform in the computation of characteristic functions and moment generating functions, instead of the usual Fourier and Laplace transforms.

Given a generic random variable u, the moment generating function (MGF) Φ_u of u is defined as the bilateral Laplace transform of the PDF of u [30], i.e.:

$$\Phi_u(s) = \mathcal{L}(p_u)(s) = \int_{-\infty}^{+\infty} p_u(u) \exp(su) du, \quad s \in \mathbb{C}, \qquad (15)$$

where $\mathcal{L}$ is the bilateral Laplace transform operator[2] on the Lebesgue space $L^1(\mathbb{R})$ [11]. The MGF is known to converge and to be analytical at least in a vertical strip of the complex

[2] Actually, the bilateral Laplace operator would involve the exponential $\exp(-su)$ [11], but, in the context of statistics, the MGF is usually defined with the exponential $\exp(su)$ as reported in Eq. (15). However, this

plane and it turns out to be implicitly related to the MoM estimation approach. In fact, if the interior of the convergence strip contains a neighborhood of the origin, then the ν-th order moment ($\nu = 1, 2, \ldots$) can be expressed as

$$m_\nu = E\{u^\nu\} = \Phi_u^{(\nu)}(0), \tag{16}$$

where the superscript denotes a differentiation operator [30]. Related quantities are the characteristic function of u, defined as the Fourier transform of the PDF, the second moment generating function Ψ_u, defined as the complex logarithm of the MGF and the ν-th order cumulant k_ν, defined as the ν-th order derivative of the second MGF computed in the origin of the complex plane:

$$\Psi_u(s) = \ln \Phi_u(s), \qquad k_\nu = \Psi_u^{(\nu)}(0). \tag{17}$$

In particular, the first and second order cumulants turn out to be equal to the distribution mean and variance, respectively [30].

The MoM estimates are actually computed by analytically expressing the moments (or the cumulants) of the parametric PDF under investigation as functions of the unknown parameters, and by estimating the moments as sample-moments, thus formulating the parameter estimation problem as the solution of a (typically non-linear) system of equations. In [25][27], this approach is specialized to non-negative random variables (such as SAR amplitude and intensity), corresponding to PDF defined on $[0, +\infty)$, by re-defining MGFs and characteristic functions as Mellin transforms and resulting in a more feasible estimation.

Thus, given a non-negative random variable u, the second-kind characteristic function ϕ_u of u is defined as the Mellin transform [38] of the PDF of u, i.e.:

$$\phi_u(s) = \mathcal{M}(p_u)(s) = \int_0^{+\infty} p_u(u) u^{s-1} du, \quad s \in \mathbb{C}, \tag{18}$$

where $\mathcal{M}$ is the Mellin transform on $L^1(0, +\infty)$. Also ϕ_u is known to converge and to be analytical in a vertical strip $\mathcal{S}$ of the complex plane [25][38]. If the interior of the convergence strip containe a neighborhood of 1, then the following definitions are formulated by analogy with the Laplace-based case [25]:

- ν-th order second kind moment: $\mu_\nu = \phi_u^{(\nu)}(1)$, $\nu = 1, 2, \ldots$;
- second kind second characteristic function: $\psi_u(s) = \ln \phi_u(s)$, $s \in \mathcal{S}$;
- ν-th order second kind cumulant: $\kappa_\nu = \psi_u^{(\nu)}(1)$, $\nu = 1, 2, \ldots$

The expressions "log-moments" and "log-cumulants" are also used for the second kind moments and cumulants, thanks to their relation with the moments of the logarithm of u, i.e.:

$$\mu_\nu = E\{(\ln u)^\nu\}, \quad \kappa_1 = \mu_1 = E\{\ln u\}, \quad \kappa_2 = \mu_2 - \mu_1^2 = \mathrm{Var}\{\ln u\}. \tag{19}$$

slight modification has no significant impact on the analytical properties of the resulting transform. Hence, hereafter we will refer to the bilateral Laplace transform as defined by Eq. (15).

Hence, the estimation method of log-cumulants is based on the analytical calculation of log-moments and log-cumulants as functions of the unknown parameters and on the inversion of the resulting equations. Hence, MoLC estimates are obtained from sample-moment estimates of the log-moments or of the log-cumulants by solving a system of non-linear equations. The numerical solution of these equations turns out to be feasible and fast for most SAR-specific distributions, such as the Nakagami-Gamma or the K ones, and the MoLC estimates also exhibit a lower variance with respect to the usual MoM ones. [25]. However, we also stress that, when dealing with non-negative random variables, the MoM approach itself can be expressed by using the Mellin transform, since

$$m_\nu = \phi_u(\nu + 1), \quad \nu = 1, 2, \dots \tag{20}$$

Therefore, if the Mellin transform of the function p_u can be computed, both the non-linear MoM equations and the MoLC ones can be derived.

3.2 MoLC parametric estimation for the GGR model

Plugging the expression (12) in the definition (18) of the Mellin transform yields:

$$\phi_r(s) = \mathcal{M}(p_r)(s) = \frac{\gamma^2 c^2}{\Gamma^2(1/c)} \int_0^{+\infty} r^s \int_0^{\pi/2} \exp[-(\gamma r)^c (|\cos\theta|^c + |\sin\theta|^c)] d\theta dr =$$

$$= \frac{\gamma^2}{\lambda^2 \Gamma^2(\lambda)} \int_0^{+\infty} r^s \int_0^{\pi/2} \exp[-(\gamma r)^{1/\lambda} A(\theta, \lambda)] d\theta dr, \quad s \in \mathbb{C} \tag{21}$$

where we have introduced the auxiliary parameter $\lambda = 1/c$ and the auxiliary function $A : [0, \pi/2] \times (0, +\infty) \to \mathbb{R}$ with $A(\theta, \lambda) = |\cos\theta|^{1/\lambda} + |\sin\theta|^{1/\lambda}$. According to the Fubini-Tonelli theorem [11], the function $(r, \theta) \longmapsto r^s \exp[-(\gamma r)^{1/\lambda} A(\theta, \lambda)]$ is Lebesgue-integrable on $[0, +\infty) \times [0, \pi/2]$, thus allowing an exchange in the order of integration, i.e.:

$$\phi_r(s) = \frac{\gamma^2}{\lambda^2 \Gamma^2(\lambda)} \int_0^{\pi/2} d\theta \int_0^{+\infty} r^s \exp[-(\gamma r)^{1/\lambda} A(\theta, \lambda)] dr. \tag{22}$$

Making the substitution $r \longmapsto \xi = (\gamma r)^{1/\lambda} A(\theta, \lambda)$ yields:

$$\phi_r(s) = \frac{\gamma^2}{\lambda^2 \Gamma^2(\lambda)} \int_0^{\pi/2} d\theta \int_0^{+\infty} \frac{\xi^{\lambda s}}{\gamma^s A(\theta, \lambda)^{\lambda s}} \exp(-\xi) \frac{\lambda \xi^{\lambda - 1}}{\gamma A(\theta, \lambda)^\lambda} d\xi =$$

$$= \frac{1}{\lambda \gamma^{s-1} \Gamma^2(\lambda)} \int_0^{+\infty} \xi^{\lambda s + \lambda - 1} \exp(-\xi) d\xi \int_0^{\pi/2} \frac{d\theta}{A(\theta, \lambda)^{\lambda s + \lambda}}. \tag{23}$$

Expressing the first integral as a Gamma function [34] eventually yields the following expression for the second kind characteristic function of the GGR model:

$$\phi_r(s) = \frac{\Gamma(\lambda s + \lambda)}{\lambda \gamma^{s-1} \Gamma^2(\lambda)} \int_0^{\pi/2} \frac{d\theta}{A(\theta, \lambda)^{\lambda s + \lambda}}. \tag{24}$$

According to Eq. (24), ϕ_r is defined in a neighborhood of 1, thus allowing the definition of log-cumulants and the consequent application of MoLC. The second kind second characteristic function turns out to be:

$$\psi_r(s) = \ln \phi_r(s) = \ln \Gamma(\lambda s + \lambda) - \ln \lambda - (s-1)\ln \gamma - 2\ln \Gamma(\lambda) + \ln \int_0^{\pi/2} \frac{d\theta}{A(\theta,\lambda)^{\lambda s+\lambda}}. \quad (25)$$

Denoting as $\Psi(\cdot)$ the digamma function [25] (i.e., the logarithmic derivative of the Gamma function) and as $\Psi(\nu,\cdot)$ the ν-th order polygamma function [25] (i.e., the ν-th order derivative of the digamma function; $\nu = 1, 2, \ldots$), we obtain:

$$\psi_r'(s) = \lambda\Psi(\lambda s + \lambda) - \ln \gamma - \lambda \int_0^{\pi/2} \frac{\ln A(\theta,\lambda)}{A(\theta,\lambda)^{\lambda s+\lambda}} d\theta \left[\int_0^{\pi/2} \frac{d\theta}{A(\theta,\lambda)^{\lambda s+\lambda}}\right]^{-1} \quad (26)$$

and

$$\psi_r''(s) = \lambda^2\Psi(1,\lambda s + \lambda) + \lambda^2 \int_0^{\pi/2} \frac{\ln^2 A(\theta,\lambda)}{A(\theta,\lambda)^{\lambda s+\lambda}} d\theta \left[\int_0^{\pi/2} \frac{d\theta}{A(\theta,\lambda)^{\lambda s+\lambda}}\right]^{-1} +$$

$$- \lambda^2 \left[\int_0^{\pi/2} \frac{\ln A(\theta,\lambda)}{A(\theta,\lambda)^{\lambda s+\lambda}} d\theta\right]^2 \left[\int_0^{\pi/2} \frac{d\theta}{A(\theta,\lambda)^{\lambda s+\lambda}}\right]^{-2}. \quad (27)$$

Introducing the function

$$G_\nu(\lambda) = \int_0^{\pi/2} \frac{\ln^\nu A(\theta,\lambda)}{A(\theta,\lambda)^{2\lambda}} d\theta, \quad \nu = 0, 1, 2, \ldots, \quad (28)$$

we obtain the following expressions for the first and the second log-cumulants:

$$\kappa_1 = \psi_r'(1) = \lambda\Psi(2\lambda) - \ln \gamma - \lambda \frac{G_1(\lambda)}{G_0(\lambda)} \quad (29)$$

$$\kappa_2 = \psi_r''(1) = \lambda^2\Psi(1,2\lambda) + \lambda^2 \frac{G_2(\lambda)G_0(\lambda) - G_1(\lambda)^2}{G_0(\lambda)^2} \quad (30)$$

MoLC first computes the following sample-mean and sample-variance estimates of κ_1 and κ_2, according to the image data $\mathcal{I} = \{r_1, r_2, \ldots, r_N\}$ [30]:

$$\hat{\kappa}_1 = \frac{1}{N}\sum_{k=1}^{N} \ln r_k, \qquad \hat{\kappa}_2 = \frac{1}{N-1}\sum_{k=1}^{N} (\ln r_k - \hat{\kappa}_1)^2 \quad (31)$$

and derives estimates $\hat{\lambda}$ and $\hat{\gamma}$ of the parameters λ and γ by solving the Eqs. (29-30). We stress that Eq. (30) does not contain γ, thus allowing to split the non-linear solution problem in two distinct stages: first, λ can be estimated by solving Eq. (30); then, the resulting estimate $\hat{\lambda}$ can be plugged into Eq. (29) to solve for γ. The second solution stage

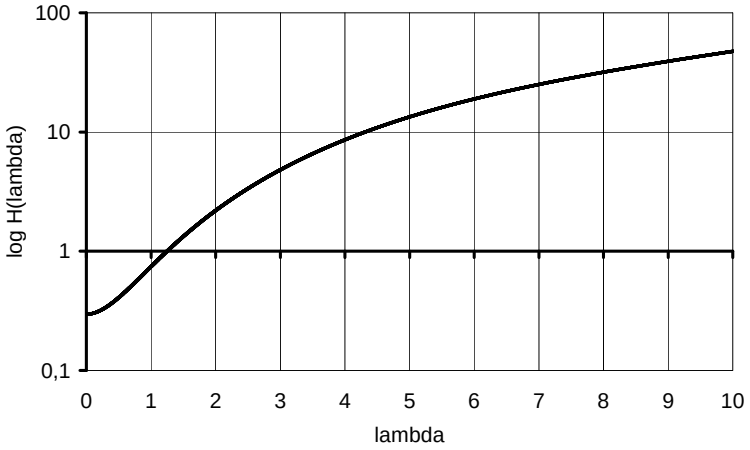


Figure 3.1: Logarithmic plot of the $H(\cdot)$ function, representing the right-hand side of Eq. (30).

can be easily carried out analytically. On the contrary, the first stage requires a numerical solution procedure. However, the function on the right-hand-side of Eq. (30), i.e.:

$$H(\lambda) = \lambda^2 \Psi(1, 2\lambda) + \lambda^2 \frac{G_2(\lambda) G_0(\lambda) - G_1(\lambda)^2}{G_0(\lambda)^2}, \quad \lambda > 0 \tag{32}$$

is stricly monotonally increasing (see Fig. 3.1), thus allowing a simple numerical solution, for instance, by means of the bisection method [4]. On the other hand, we note that applying MoM would involve computing the first two moments m_1 and m_2 (i.e., letting $s = 2$ and $s = 3$ in Eq. (24), respectively), thus leading to more complicated numerical computations.

As shown in Fig. 3.1, the $H(\cdot)$ function is lower bounded, i.e., $H(\lambda) \geq H^* \simeq 0.296$ for all $\lambda > 0$. Hence, if $\hat{\kappa}_2 < H^*$ the equation $H(\lambda) = \hat{\kappa}_2$ has no solution. In this case, the GGR model turns out not to be compatible with the empirical data distribution.

3.3 Consistency of the proposed estimator

We study here the asymptotic properties of the previously introduced estimator, specifically proving its consistency. Since the estimation procedure involves explicitly the parameter $\lambda = 1/c$ instead of c itself, without loss of generality we refer to (λ, γ), and not to (c, γ), as the parameter vector of the GGR distribution. Dealing with the asymptotic behavior, we assume the availability of a random sequence $\{r_n\}_{n=1}^{\infty}$ of i.i.d. data samples, drawn according to a GGR distribution. We denote as $\Theta : (0, +\infty)^2 \to \mathbb{R}^2$ the non-linear transformation mapping a parameter vector $\xi = (\lambda, \gamma)$ to the resulting log-cumulant vector $\kappa = (\kappa_1, \kappa_2)$, i.e.:

$$\Theta(\lambda, \gamma) = \left(\lambda \Psi(2\lambda) - \ln \gamma - \lambda \frac{G_1(\lambda)}{G_0(\lambda)},\ H(\lambda) \right) \tag{33}$$

Hence, denoting as $\xi^* = (\lambda^*, \gamma^*)$ the true parameter vector, the resulting true log-cumulants of the data distribution are the components of the vector $\kappa^* = \Theta(\xi^*) = \Theta(\lambda^*, \gamma^*)$. These log-cumulants are estimated according to the data $\{r_n\}_{n=1}^{\infty}$, by introducing the sequence $\{\hat{\kappa}_n = (\hat{\kappa}_{1n}, \hat{\kappa}_{2n})\}_{n=1}^{\infty}$ of sample-mean and sample-variance estimates, i.e.:

$$\hat{\kappa}_{1n} = \frac{1}{n}\sum_{k=1}^{n} \ln r_k, \qquad \hat{\kappa}_{2n} = \frac{1}{n-1}\sum_{k=1}^{n} (\ln r_k - \hat{\kappa}_1)^2 \tag{34}$$

Thanks to the strict monotonicity of $H(\cdot)$ and to the invertibility of Eq. (29) with respect to γ, $\Theta(\cdot)$ is an invertible mapping, thus yielding, for any $n = 1, 2, \ldots$, a unique solution $\hat{\xi}_n = (\hat{\lambda}_n, \hat{\gamma}_n) = \Theta^{-1}(\hat{\kappa}_n)$ of the vector equation $\Theta(\xi_n) = \hat{\kappa}_n$. In addition, both Θ and its inverse Θ^{-1} turn out to be continuous mapping, Θ^{-1} being, in particular, continuous at κ^*. Therefore, for any $\varepsilon > 0$ there exists $\delta_\varepsilon > 0$, such that[3] $||\kappa - \kappa^*||_2 < \delta_\varepsilon$ yields $||\Theta^{-1}(\kappa) - \xi^*||_\infty < \varepsilon$. Hence, if $||\hat{\kappa}_n - \kappa^*||_2 < \delta_\varepsilon$, then $||\hat{\xi}_n - \xi^*||_\infty < \varepsilon$, which yields the following relation between events:

$$\{||\hat{\kappa}_n - \kappa^*||_2 < \delta_\varepsilon\} \subset \{||\hat{\xi}_n - \xi^*||_\infty < \varepsilon\} \tag{35}$$

Therefore:

$$P\{|\hat{\lambda}_n - \lambda^*| < \varepsilon, |\hat{\gamma}_n - \gamma^*| < \varepsilon\} = P\{||\hat{\xi}_n - \xi^*||_\infty < \varepsilon\} \geq P\{||\hat{\kappa}_n - \kappa^*||_2 < \delta_\varepsilon\} \tag{36}$$

Applying first the Markov inequality to the non-negative random variable $||\hat{\kappa}_n - \kappa^*||_2$ [30] and then the Cauchy-Schwartz inequality [30], we have:

$$P\{||\hat{\kappa}_n - \kappa^*||_2 < \delta_\varepsilon\} \geq 1 - \frac{E\{||\hat{\kappa}_n - \kappa^*||_2\}}{\delta_\varepsilon} \geq 1 - \frac{E\{||\hat{\kappa}_n - \kappa^*||_2^2\}^{1/2}}{\delta_\varepsilon} \tag{37}$$

Therefore:

$$P\{|\hat{\lambda}_n - \lambda^*| < \varepsilon, |\hat{\gamma}_n - \gamma^*| < \varepsilon\} \geq 1 - \frac{E\{||\hat{\kappa}_n - \kappa^*||_2^2\}^{1/2}}{\delta_\varepsilon} =$$

$$= 1 - \frac{E\{(\hat{\kappa}_{1n} - \kappa_1^*)^2 + (\hat{\kappa}_{2n} - \kappa_2^*)^2\}}{\delta_\varepsilon} \tag{38}$$

The sample-mean estimate $\hat{\kappa}_{1n}$ of $\kappa_1 = E\{\ln r\}$ and the sample-variance estimate $\hat{\kappa}_{2n}$ of $\kappa_2 = \mathrm{Var}\{\ln r\}$, are known to be unbiased, with variances given by [30]:

$$\mathrm{Var}\{\hat{\kappa}_{1n}\} = \frac{\kappa_2}{n}, \qquad \mathrm{Var}\{\hat{\kappa}_{2n}\} = \frac{1}{n}\left(\beta - \frac{n-3}{n-1}\kappa_2^2\right) \tag{39}$$

[3] We denote here as $||\cdot||_2$ and as $||\cdot||_\infty$ the Euclidean and the Tchebitchev (i.e., uniform) norm on $\mathbb{R}^2$, respectively [11]. Adopting the former in the domain of the mapping Θ^{-1} and the latter in the co-domain is advantageous in the calculations and involves no loss of generality, since all norms on a finite-dimensional vector space are equivalent [11].

where $\beta = E\{(\ln r - \kappa_1)^4\}$. Therefore:

$$P\{|\hat{\lambda}_n - \lambda^*| < \varepsilon, |\hat{\gamma}_n - \gamma^*| < \varepsilon\} \geq 1 - \frac{\mathrm{Var}\{\hat{\kappa}_{1n}\} + \mathrm{Var}\{\hat{\kappa}_{2n}\}}{\delta_\varepsilon}$$

$$= 1 - \frac{1}{n\delta_\varepsilon}\left(\kappa_2 + \beta - \frac{n-3}{n-1}\kappa_2^2\right) \tag{40}$$

We finally conclude that:

$$\lim_{n \to +\infty} P\{|\hat{\lambda}_n - \lambda^*| < \varepsilon, |\hat{\gamma}_n - \gamma^*| < \varepsilon\} = 1 \tag{41}$$

which proves the random vector sequence $\{(\hat{\lambda}_n, \hat{\gamma}_n)\}_{n=1}^{\infty}$ to converge in probability to the true parameter vector (λ^*, γ^*). Hence, the developed MoLC estimator for the proposed GGR distribution turns out to be consistent [41].

4 Experimental results

4.1 Data sets for experiments

The proposed parametric GGR model, endowed with the MoLC estimation strategy described in Section 3, have been tested on 10 real SAR images, and compared with several previously developed statistical models for the SAR backscattering phenomena. The first six images used for experiments are single bands acquired in August 1989 on the agricultural region of Feltwell (UK) by a fully polarimetric PLC-band NASA/JPL airborne sensor [35]. Specifically, all the three polarizations (HH, HV, VV) acquired at band C, the HV and VV polarizations acquired at band L and the HH polarization acquired at band P have been used. The remaining channels (namely, L-HH, P-HV, and P-VV) have been discarded, since their histograms exhibit strong irregularities (see, for instance, Fig. 4.1), probably due to the underlying calibration and registration processes. Hereafter, the adopted Feltwell bands will be denoted synthetically as "Feltwell-CHH", "Feltwell-CHV", ..., "Feltwell-PHH".

The other four employed images are:

- a single-look ERS-1 image, acquired in April 1993 on the urban and agricultural region around Bourges (France);
- an ERS-1 image of the agricultural region of Flevoland (Netherlands);
- a 3-look XSAR scene of portion of the Swiss territory, comprising a mountain zone, a portion of a lake, and a urban area [7];
- a 3-look ESAR image of the area of Oberpfaffenhofen near Munich (Germany).

All the employed images are shown in Appendix A, after histogram stretching and/or equalization.

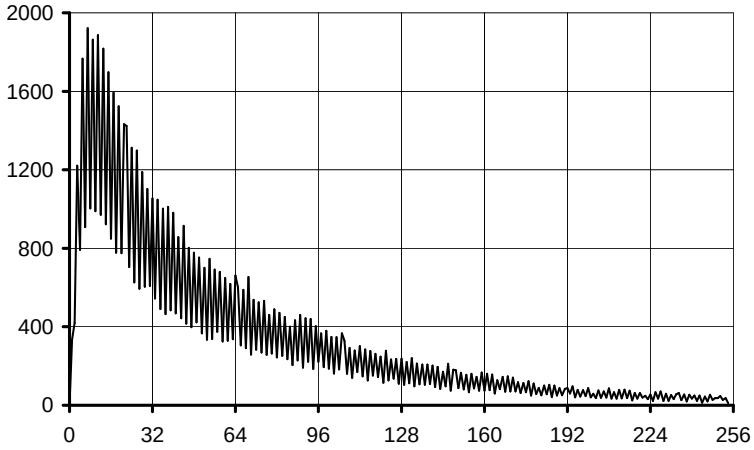


Figure 4.1: Plot of the histogram of the HH polarization acquired at band L for the "Feltwell" data set, highlighting the presence of an irregular "zig-zag" behavior of the histogram itself.

4.2 PDF estimation results

In order to assess the effectiveness of the proposed parametric PDF estimation algorithm, we have applied the method to the above-mentioned 10 images, evaluating the estimation results both qualitatively (by means of a visual comparison between the estimated PDF and the empirical data distribution, i.e., the image histogram) and quantitatively (i.e., by computing the correlation coefficient between the estimated PDF and the histogram itself).

The results have been compared with the ones provided by several previously developed parametric models for the SAR backscattering phenomena. Specifically dealing with amplitude images, we have involved in the comparison the Nakagami distribution, the SαS generalized Rayleigh distribution (hereafter denoted simply as SαSGR) and the amplitude PDF (7) corresponding to K-distributed intensities (hereafter denoted as "K-root"). We do not consider explicitly in the comparison the Rayleigh PDF, since it is a particular case of all the above-mentioned models. For all considered parametric families the MoLC estimation strategy has been adopted, both for homogeneity with respect to GGR and thanks to the good estimation properties this algorithm has been proved to exhibit, for instance for the Nakagami-Gamma model [25]. The resulting correlation-coefficients are shown in Table 4.1

The GGR model turns out to be well-defined (i.e., the empirical sample-variance $\hat{\kappa}_2$ satisfies the condition $\hat{\kappa}_2 \geq H^*$) for all considered images except "Flevoland" and "Oberpfaffenhofen". In all cases in which GGR fitting is feasible, except "Bourges", the quantitative correlation coefficients suggest this parametric estimation approach to better fit the data histograms than the other considered parametric scattering models. A visual comparison between the histograms and the plots of the estimated PDFs actually confirms this conclusion. As an example, we show in Fig. 4.2 the results obtained for "Feltwell-CHH" and we list in Appendix B all the plotted results.

Image	Parametric model			
	GGR	Nakagami	SαSGR	K-root
Feltwell-CHH	99,42%	95,80%	89,98%	not defined
Feltwell-CHV	98,95%	97,13%	88,87%	not defined
Feltwell-CVV	99,11%	94,56%	87,54%	not defined
Feltwell-LHV	98,74%	94,14%	75,55%	not defined
Feltwell-LVV	99,28%	93,43%	84,96%	not defined
Feltwell-PHH	98,61%	92,54%	81,57%	not defined
Bourges	98,97%	98,97%	95,57%	99,77%
Flevoland	not defined	98,70%	88,32%	99,77%
Suisse-Lake	99,63%	97,90%	94,30%	not defined
Oberpfaffenhofen	not defined	99,88%	91,00%	99,86%

Table 4.1: Correlation coefficients between the estimated PDFs and the image histograms for all considered parametric families and all employed SAR images.

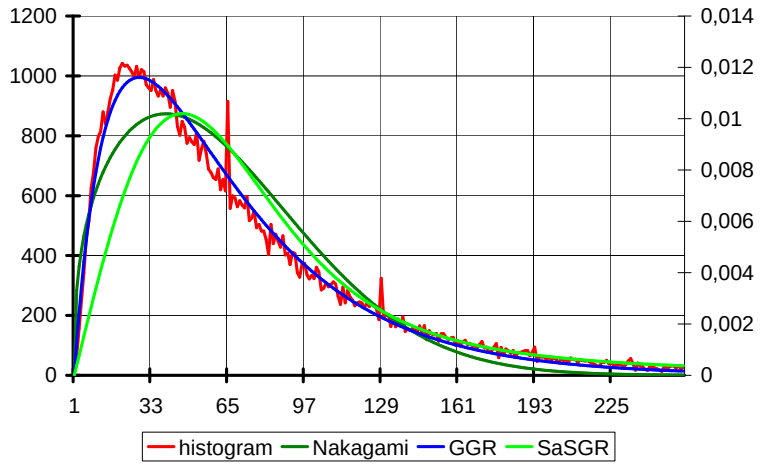


Figure 4.2: Plot of the image histogram and of the estimated GGR, SαSGR, and Nakagami PDFs for the "Feltwell-CHH" data set.

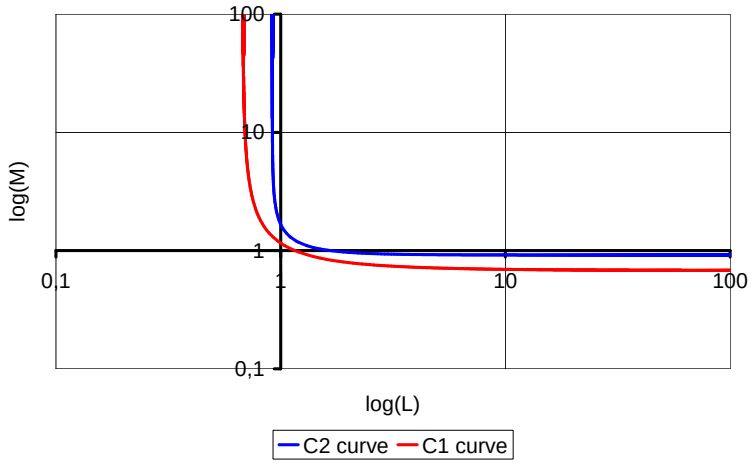


Figure 4.3: Logarithmic plot of the curves $\mathcal{C}_1$ and $\mathcal{C}_2$ for K-root parameter estimation applied to the "Feltwell-CHH" image.

It is interesting to stress that it is possible to fit the K-root model only to "Bourges", "Oberpfaffenhofen", and "Flevoland". In fact, as with GGR, the system of non-linear equations to be solved in order to compute the parameter estimates for K-root can have no solutions for specific combinations of the values of the sample-log-cumulants. In particular, the MoLC estimates $\hat{\lambda}, \hat{L}$, and $\hat{M}$ of the parameters λ, L, and M of the K-root PDF (7) are computed by solving the following equations [24]:

$$2\hat{\kappa}_1 = -2\ln\hat{\lambda} + \Psi(\hat{L}) - \ln\hat{L} + \Psi(\hat{M}) - \ln\hat{M} \tag{42}$$

$$4\hat{\kappa}_2 = \Psi(1,\hat{L}) + \Psi(1,\hat{M}) \tag{43}$$

$$8\hat{\kappa}_3 = \Psi(2,\hat{L}) + \Psi(2,\hat{M}), \tag{44}$$

where $\hat{\kappa}_1, \hat{\kappa}_2$, and $\hat{\kappa}_3$ are sample-moment estimates of the log-cumulants κ_1, κ_2, and κ_3 respectively. However, the joint system of equations (43-44), which yields the estimates of the parameters L and M, can have no solutions, since the curves $\mathcal{C}_1 : 4\hat{\kappa}_2 = \Psi(1,\hat{L}) + \Psi(1,\hat{M})$ and $\mathcal{C}_2 : 8\hat{\kappa}_3 = \Psi(2,\hat{L}) + \Psi(2,\hat{M})$ in the $(\hat{L},\hat{M})$ plane can have empty intersection. In fact, according to the monotonicity and asymptotic properties[4] of both $\Psi(1,\cdot)$ and $\Psi(2,\cdot)$, standard calculus allows proving that both $\mathcal{C}_1$ and $\mathcal{C}_2$ lie in the positive quadrant $L > 0, M > 0$ and exhibit a "hyperpolic" shape, with both a horizontal and a vertical asymptotic line. However, these two curves can have no intersection, as in the example shown in Fig. 4.3.

[4]In particular, $\Psi(1,\cdot)$ is a strictly decreasing function on $(0,+\infty)$, vanishing at infinity and positively diverging at the origin, whereas $\Psi(2,\cdot)$ is strictly increasing on $(0,+\infty)$, vanishing at infinity and negatively diverging at the origin [24].

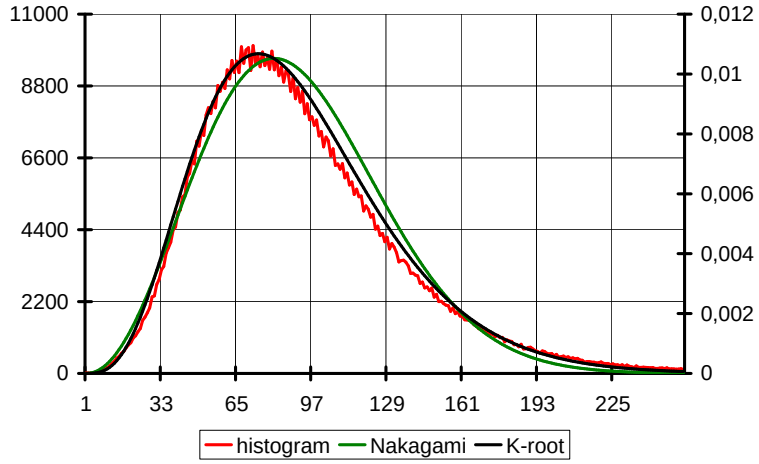


Figure 4.4: Plot of the image histogram and of the estimated Nakagami and K-root PDFs for the "Flevoland" data set.

However, the experiments suggest a complementarity between the proposed GGR model and the usual K-root one, since for all images except "Bourges" only one of the two parametric PDFs turns out to be feasible. In particular, the histogram of "Flevoland" is characterized by a poor content at low grey-level values, and "Oberpfaffenhofen" has a very small dynamics range, both conditions yielding too low values of the empyrical sample-variance of the logarithm of the grey-levels to allow the application of GGR. However, in both cases, K-root performs very well in fitting the histogram of these images, both from the viewpoint of the correlation coefficient (see Table 4.1) and from the viewpoint of the visual comparison between the histogram and the estimated PDF (see, for instance, Fig. 4.4). Furthermore, for the "Bourges" image, which allows the application of both models, the results provided by GGR and by K-root are both good and quite similar (see Fig. 4.5). On the contrary, as highlighted by Table 4.1 and as shown by the PDF plots shown in Appendix B, both Nakagami and SαSGR yields worse estimation performances, thus proving to be less effective amplitude PDF models than GGR and K-root.

We note that, when the image histogram exhibits a very "peaky" distribution, such as in the "Feltwell-LHV" case (see Fig. 4.6), although providing the best estimation performaces among the considered backscattering models (see Table 4.1), GGR yields a visually biased result, not accurately modelling the narrow peak of the distribution. In order to improve the estimation accuracy for such "peaky" distributions, an even higher flexibility of the estimation model would be required, for instance, by further generalizing GGR by admitting different values for the parameters c and γ of the two generalized Gaussian components of the complex backscattered signal.

An analysis of the parameter estimates computed by MoLC for the 8 images for which GGR is well-defined (see Table 4.2) stresses the usefulness of the proposed generalized Gaus-

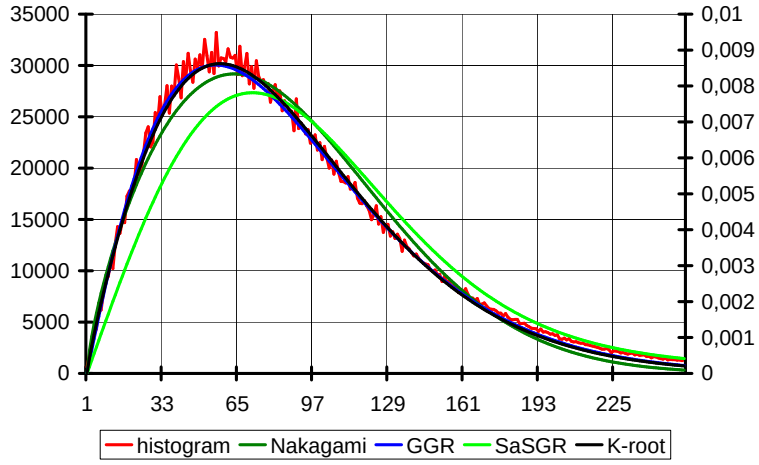


Figure 4.5: Plot of the image histogram and of the estimated GGR, K-root, SαSGR, and Nakagami PDFs for the "Bourges" data set.

sian backscattering model with respect to the usual Gaussian one. For all images, the estimate $\hat{c} = 1/\hat{\lambda}$ of the shape parameter c turned out to be far lower than 2 (often even lower than 1), thus highlighting a strongly non-Gaussian behavior of the backscattering signal and stressing the need to take into account the presence of heavy distribution tails. It is also interesting to note that the estimate $\hat{\gamma}$ of the γ parameter exhibits for "Feltwell-LHV" and for "Feltwell-PHH" much higher values than for the other images. This may be interpreted as a consequence of the fact that both "Feltwell-LHV" and "Feltwell-PHH" exhibit the above mentioned "peaky" behavior in the data distribution, thus presenting a proportionally lower variance with respect to the other images. Plugging the expression (24) of the second kind characteristic function of the GGR PDF in the relation (20) between the moments and the Mellin transform, we obtain $\mathrm{Var}\{r\} = m_2 - m_1^2 = \phi_r(3) - \phi_r(2)^2 \propto \gamma^{-2}$. Therefore, for images characterized by a "peaky" histogram, $\mathrm{Var}\{r\}$ has a low value and so a correspondingly high value is expected for the parameter γ.

5 Conclusions

In this research report an innovative parametric model has been proposed to characterize the statistics of the backscattering phenomena generating a SAR image. Specifically, a closed form has been derived for the resulting amplitude parametric PDF and a parameter estimation algorithm, based on the Mellin transform and on the method of log-cumulants, has been developed and tested on several real XSAR, ESAR, ERS-1 and airborne SAR images.

Image	$\hat{c}$	$\hat{\gamma}$
Feltwell-CHH	0,8576	0,0322
Feltwell-CHV	0,6903	0,0506
Feltwell-CVV	0,7633	0,0444
Feltwell-LHV	0,3683	1,0947
Feltwell-LVV	0,6032	0,0931
Feltwell-PHH	0,4635	0,4817
Bourges	1,3722	0,0132
Suisse-Lake	1,0376	0,0271

Table 4.2: Parameter estimates provided by MoLC (with $\hat{c} = 1/\hat{\lambda}$) for the proposed GGR model, applied to each considered image. "Flevoland" and "Oberpfaffenhofen" are not reported here, since the estimation process yields no solution for these images (see Table 4.1).

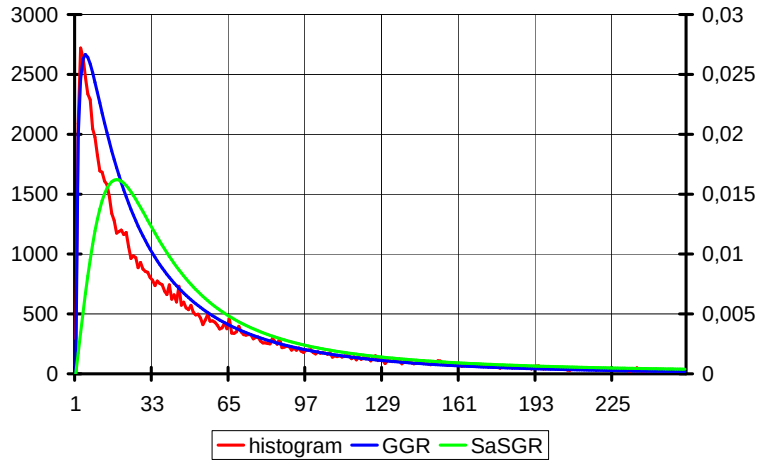


Figure 4.6: Plot of the image histogram and of the estimated GGR and SαSGR PDFs for the "Feltwell-LHV" data set.

The numerical experiments prove the proposed method to outperform the majority of the previously proposed approaches to SAR backscattering parametric modelling, namely, the Nakagami-Gamma model, the K distribution and the "heavy-tailed" SαS generalized Rayleigh distribution. Specifically, the PDF estimates generated by the proposed GGR model almost always achieve higher correlation coefficients with the image histograms than the above-mentioned models, also exhibiting a better visual fit between the estimates and the histogram themselves. Accurate results have been obtained, in particular, for images acquired by several different SAR sensors, namely ESAR, XSAR, ERS-1 and the NASA/JPL airborne SAR sensor, thus proving the proposed parametric algorithm to be a flexible and effective estimation tool. We stress, in particular, that good estimation accuracies have also been obtained for multilook SAR data, although multilooking issues are not explicitly addressed in the theoretical development of the proposed algorithm, thus confirming its flexibility and applicability to a large variety of radar images.

However, a visually biased estimate is obtained for very "peaky" empirical distributions, thus suggesting, as a possible development, a further generalization of the proposed model, for instance by assuming different values for the parameters of the generalized Gaussian distributions characterizing the real and the imaginary components of the complex backscattered signal. Such a choice would yield, in fact, an even larger modelling flexibility, although at the expense of a much more complicated parameter estimation process.

However, the method turns out not to be feasible for all considered images, since the estimation process can yield no solution for specific combinations of the values of the sample-log-cumulants. Anyway, from this viewpoint, the experiments suggest a complementarity between the proposed model and the K distribution, since, for almost all the considered images, only one of these two models can be feasibly estimated. In addition, the resulting GGR or K model always better fit the image histogram with respect to Nakagami-Gamma or to SαS generalized Rayleigh. In any case, the experiments have suggested GGR to have a larger applicability than the K distribution, since GGR has turned out to be feasible for 8 of the 10 employed images, whereas the K-distribution is feasible for only 3 images. As a future development of this activity, this observed complementarity may be further exploited by performing a pre-analysis of the image histogram in order to automatically check the feasibility of GGR and of the K model and, in case of joint applicability of both PDFs, in order to select the optimal model for the input SAR image.

All the considered parametric estimation strategies exhibit very short computational times, since the non-linear equations provided by the method of log-cumulants can be easily, for instance, solved by using a simple bisection method. In particular, the K model involves the numerical solution of a system of two non-linear equations, whereas the other three parametric families involve, at most, the numerical solution of a single equation [25]. However, as discussed in [24], the numerical computations required by the K model are not critical, thus not involving significantly longer estimation times than the other three PDFs.

In any case, a further reduction of the computation time for GGR could be obtained by specifically optimizing the numerical computation of the PDF expression and of the $G_\nu(\cdot)$ function ($\nu = 0, 1, 2$). In the current research work, in fact, standard numerical integration

techniques [32] have been used to compute the integral involved by this quantities. As with the usual special functions (e.g.: the Gamma or the Bessel function), we expect a computational time reduction if adopting more sophisticated numerical strategies, such as case-specific series expansions [32]. Finally, we stress that the computation time is almost independent of the image size, since the sample-log-cumulants can be computed by directly employing the image histogram. Hence, the number of pixels in the image only influences the time needed to compute this histogram, but not the time required to estimate the values of the parameters which optimally fit the histogram itself.

Acknowledgments

This research was carried out within the framework of the IMAVIS project which was funded by the European Union (EU). The support is gratefully acknowledged. The authors would also like to thank the French Space Agency CNES and the French Research Center CESBIO which provided the "Bourges", "Flevoland", "Suisse-Lake", and "Oberpfaffenhofen" data sets, available on the CD-ROM "Speckle filters compararative tests" (©CNES, 2001).

Appendix

A SAR images employed for experiments

This appendix shows the 10 images employed in the experiments (Figs. A.1-A.10). Only for visualization purposes, their histograms have been stretched and/or equalized.

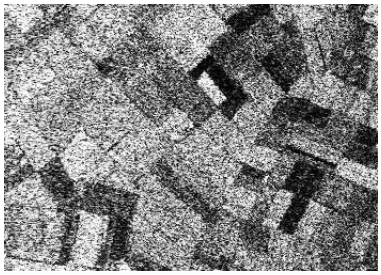


Figure A.1: "Feltwell-CHH" image.

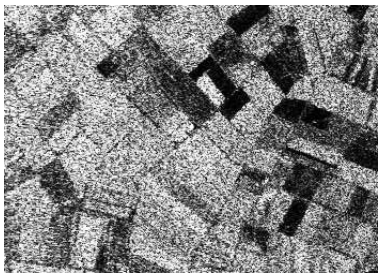


Figure A.2: "Feltwell-CHV" image.

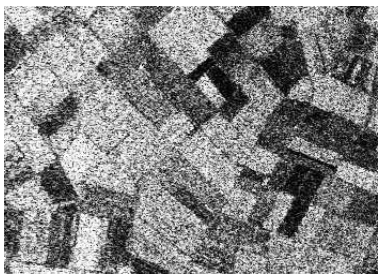


Figure A.3: "Feltwell-CVV" image.

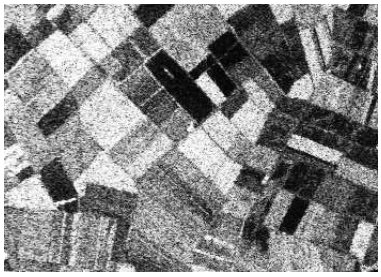


Figure A.4: "Feltwell-LHV" image.

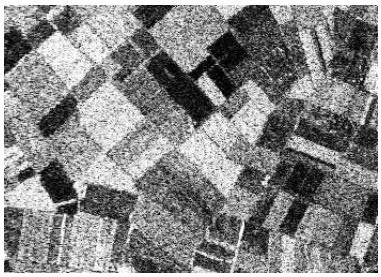


Figure A.5: "Feltwell-LVV" image.

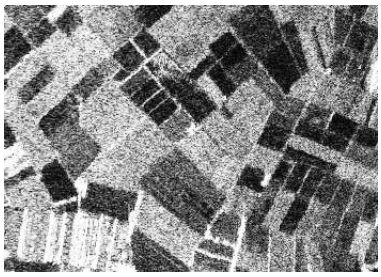


Figure A.6: "Feltwell-PHH".

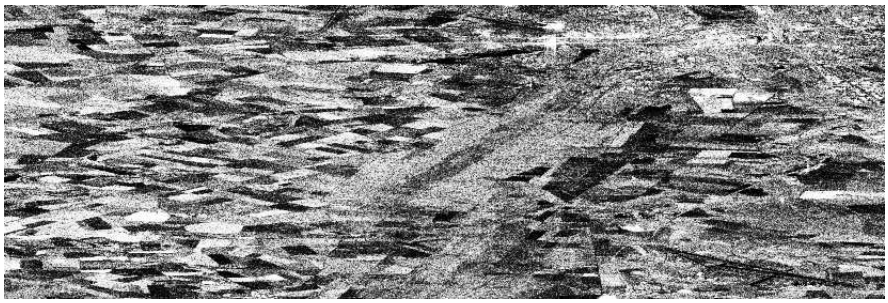


Figure A.7: "Bourges".



Figure A.8: "Flevoland" image.

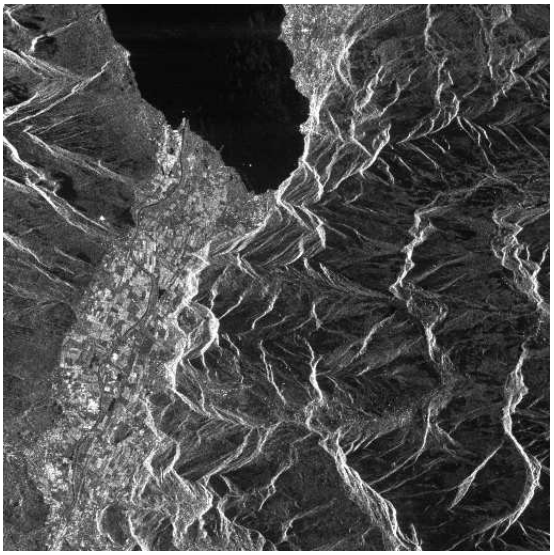


Figure A.9: "Suisse-Lake" image.

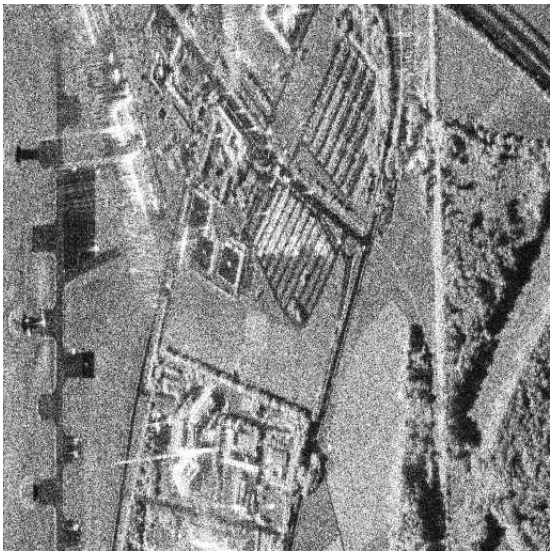


Figure A.10: "Oberpfaffenhofen" image.

B Plots of the estimated PDFs

In this appendix we report the estimated PDFs provided by MoLC applied to each parametric family involved in the experiments presented in Section 4 (Figs. B.1-B.10), together with the histograms of the corresponding images.

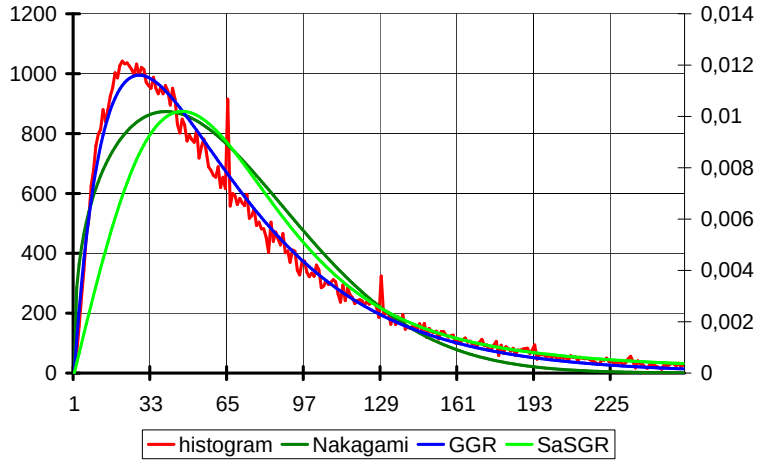


Figure B.1: Plot of the image histogram and of the estimated PDFs for the "Feltwell-CHH" data set.

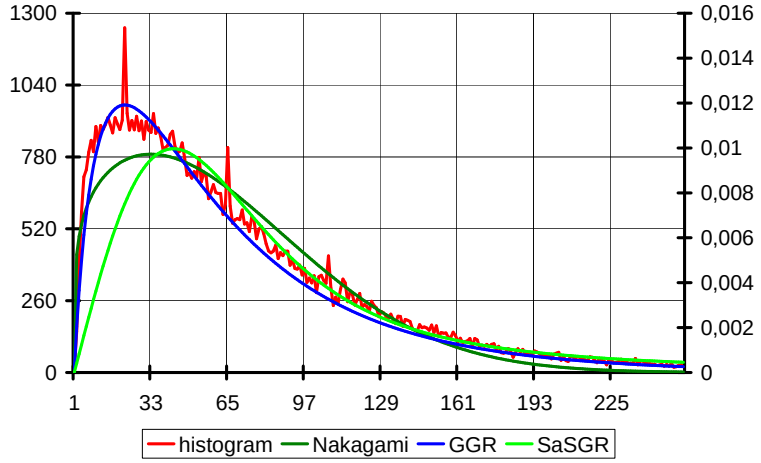


Figure B.2: Plot of the image histogram and of the estimated PDFs for the "Feltwell-CHV" data set.

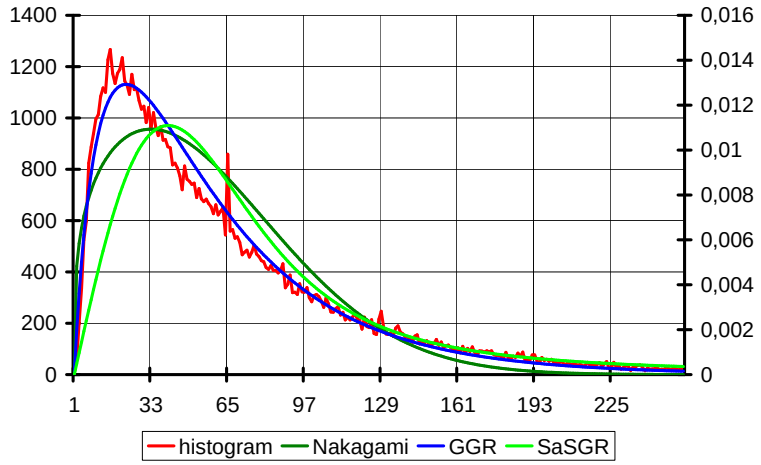


Figure B.3: Plot of the image histogram and of the estimated PDFs for the "Feltwell-CVV" data set.

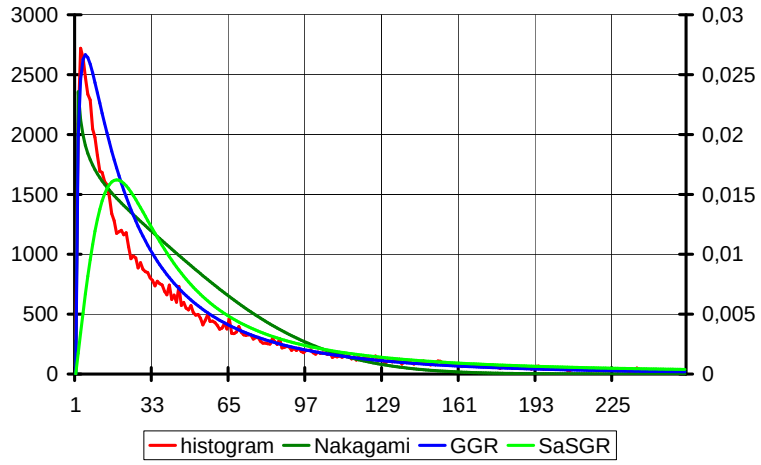


Figure B.4: Plot of the image histogram and of the estimated PDFs for the "Feltwell-LHV" data set.

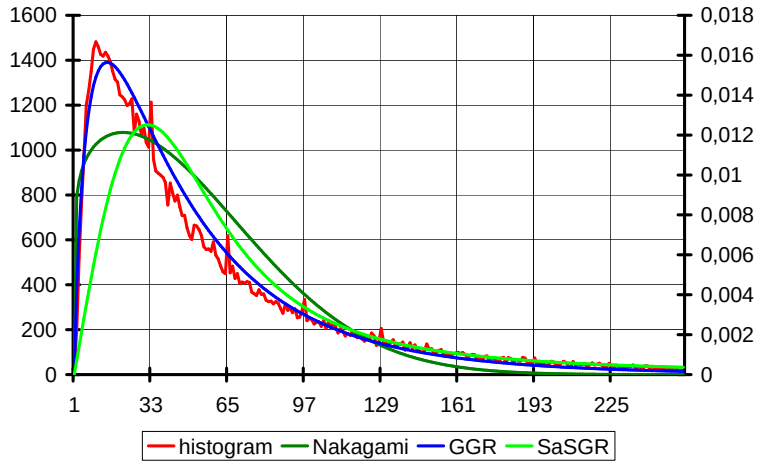


Figure B.5: Plot of the image histogram and of the estimated PDFs for the "Feltwell-LVV" data set.

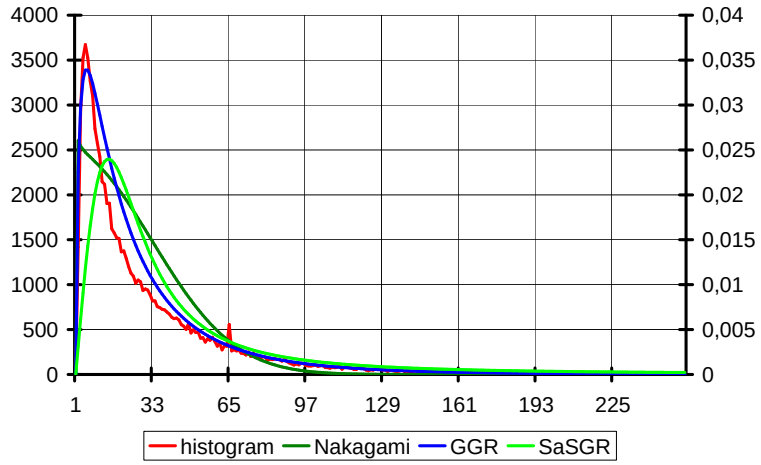


Figure B.6: Plot of the image histogram and of the estimated PDFs for the "Feltwell-PHH" data set.

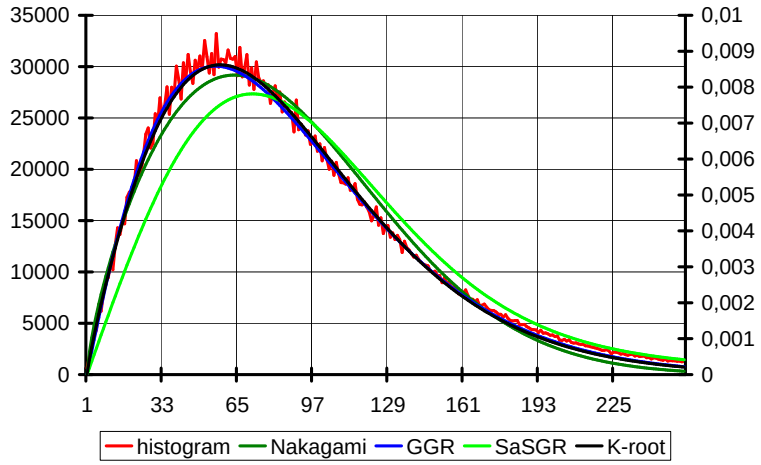


Figure B.7: Plot of the image histogram and of the estimated PDFs for the "Bourges" data set.

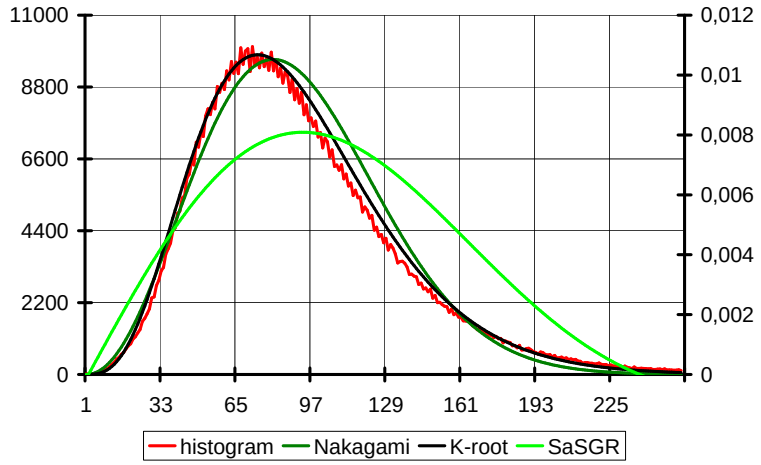


Figure B.8: Plot of the image histogram and of the estimated PDFs for the "Flevoland" data set.

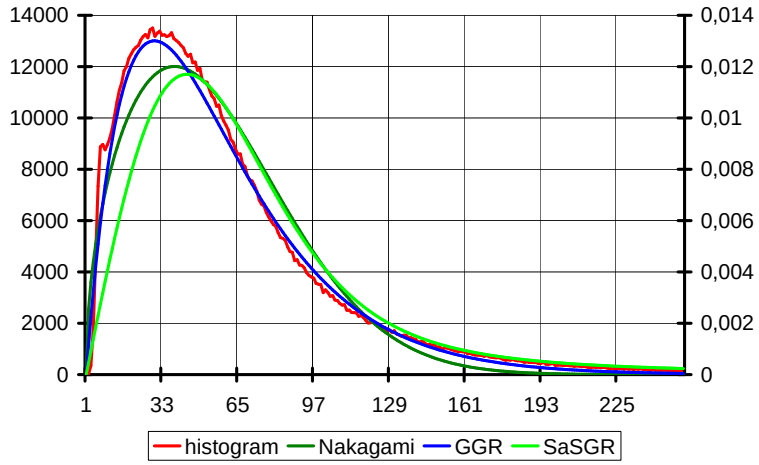


Figure B.9: Plot of the image histogram and of the estimated PDFs for the "Suisse-Lake" data set.

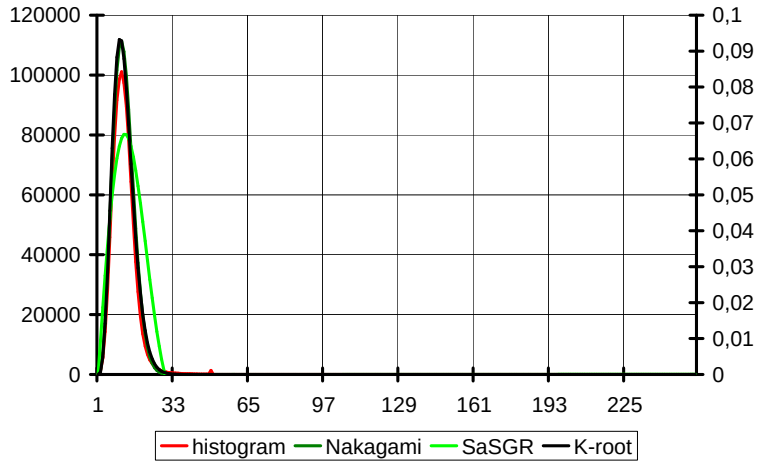


Figure B.10: Plot of the image histogram and of the estimated PDFs for the "Oberpfaffenhofen" data set.

References

[1] C. M. Bishop, *Neural networks for pattern recognition*, 2nd edition, Oxford University Press, 1996.

[2] C. Bouman and K. Sauer, *A generalized Gaussian image model for edge-preserving map estimation*, IEEE Transactions on Image Processing **2** (1993), 296–310.

[3] F. Bowman, *Introduction to Bessel functions*, Dover Publications, New York, 1968.

[4] O. Caligaris and P. Oliva, *Analisi matematica I*, 2nd edition ECIG, Genova (in italian), 1994.

[5] M. Cheney, *A mathematical tutorial on synthetic aperture radar*, SIAM Review **43** (2001), no. 2.

[6] ———, *An introduction to synthetic aperture radar (SAR) and SAR interferometry*, pp. 167–177, in "Approximation theory X: wavelets, splines, and applications", C. K. Chui, L. L. Schumacher, and J. Stockler editors, Vanderbilt University Press, Nashville, TN, U.S.A., 2002.

[7] M. Datcu, K.Seidel, and M. Walessa, *Spatial information retrieval from remote sensing images: Part I. information theoretical perspective*, IEEE Transactions on Geoscience and Remote Sensing **36** (1998), 1431–1445.

[8] Y. Delignon and W. Pieczynski, *Modelling non-Rayleigh speckle distribution in SAR images*, IEEE Transactions on Geoscience and Remote Sensing **40** (2002), no. 6, 1430–1435.

[9] R. O. Duda, P. E. Hart, and D. G. Stork, *Pattern classification*, 2nd edition, Wiley, New York, 2001.

[10] K. Fukunaga, *Introduction to statistical pattern recognition*, 2nd edition, Academic Press, 1990.

[11] G. Gilardi, *Analisi tre*, McGraw-Hill Italia, Milano (in italian), 1994.

[12] E. Jakeman and P. N. Pusey, *A model for non-Rayleigh sea echo*, IEEE Transactions on Antennas and Propagation **24** (1976), 806–814.

[13] ———, *Significance of K distributions in scattering experiments*, Phys. Rev. Lett. **40** (1978), 546–550.

[14] I.-R. Joughin, D. P. Winebrenner, and D. B. Percival, *Probability density functions for multilook polarimetric signatures*, IEEE Transactions on Geoscience and Remote Sensing **32** (1994), no. 3.

[15] G. K. Karagiannidis, D. A. Zogas, and S. A. Kotsopoulos, *On the multivariate Nakagami-m distribution with exponential correlation*, IEEE Transactions on Communications **51** (2003), no. 8, 1240–1244.

[16] E. E. Kuruoglu, *Density parameter estimation of skewed alpha-stable distributions*, IEEE Transactions on Signal Processing **49** (2001), no. 10, 2192–2201.

[17] E. E. Kuruoglu and J. Zerubia, *Modelling SAR images with a generalization of the Rayleigh distribution*, Research Report 4121, INRIA, February 2001.

[18] ———, *Skewed α-stable distributions for modelling textures*, Pattern Recognition Letters **24** (2003), 339–348.

[19] J.-S. Lee, K. W. Hoppel, S. A. Mango, and A. R. Miller, *Intensity and phase statistics of multilook polarimetric and interferometric SAR imagery*, IEEE Transactions on Geoscience and Remote Sensing **32** (1994), no. 5.

[20] P. Levy, *Calcul des probabilites*, Gauthiers-Villars (in french), Paris, 1925.

[21] S. Mallat, *A wavelet tour of signal processing*, Academic Press, 1999.

[22] P. Mantero, G. Moser, and S. B. Serpico, *Partially supervised classification of remote sensing images using svm-based probability density estimation*, IEEE honorary workshop for Prof. D. A. Landgrebe, 27-28 October 2003 (in press), 2003.

[23] P. Moulin and J. Liu, *Analysis of multiresolution image denoising schemes using generalized Gaussian and complexity priors*, IEEE Trans. on Information Theory **45** (1999), 909–919.

[24] J. M. Nicolas, *Introduction aux statistiques de deuxième espéce: application aux lois d'images RSO (introduction to second kind statistics: applications to SAR images laws)*, Research Report (in french) 2002D001, ENST, Paris, February 2002.

[25] J.-M. Nicolas, *Introduction aux statistiques de deuxième espéce: applications des log-moments et des log-cumulants a l'analyse des lois d'images radar*, Traitement du Signal (in french) **19** (2002).

[26] J.-M. Nicolas and A. Maruani, *Lower-order statistics: a new approach for probability density functions defined on* $\mathbb{R}^+$, Proceedings of the EUSIPCO Conference, Tampere (Finland), 2000.

[27] J.-M. Nicolas and F. Tupin, *Gamma mixture modeled with "second kind statistics": application to sar image processing*, Proceedings of the IGARSS Conference, Toronto (Canada), 2002.

[28] C. Oliver and S. Quegan, *Understanding synthetic aperture radar images*, Artech House, Norwood, 1998.

[29] C. J. Oliver, *Correlated K-distributed scattering model*, Opt. Acta **32** (1985), 1515–1547.

[30] A. Papoulis, *Probability, random variables, and stochastic processes*, 3rd edition, McGraw-Hill International Editions, 1991.

[31] E. Parzen, *On estimation of probability density function and mode*, Signal Processing **33** (1962), 267–281.

[32] W. H. Press, S. A. Teukolsky, W. T. Wetterling, and B. P. Flannery, *Numerical recipes in C*, Cambridge University Press, Cambridge, 2002.

[33] J.A. Richards and X. Jia, *Remote sensing digital image analysis*, Springer-Verlag, Berlin, 1999.

[34] W. Rudin, *Principles of mathematical analysis*, 2nd edition, McGraw-Hill, 1976.

[35] S. B. Serpico, L. Bruzzone, and F. Roli, *An experimental comparison of neural and statistical non-parametric algorithms for supervised classification of remote sensing images*, Pattern Recognition Letters **17** (1996), 1331–1341.

[36] E. P. Simoncelli, *Statistical models for images: compression restoration and synthesis*, Proceedings of the Asilomar Conference on Signals, Systems and Computers, Lausanne (Switzerland), vol. 1, 1997, pp. 673–678.

[37] E. P. Simoncelli and E. H. Adelson, *Noise removal via Bayesian wavelet coring*, Proceedings of the Third IEEE International Conference on Image Processing, vol. 1, 1996, pp. 379–382.

[38] I. Sneddon, *The use of integral transforms*, McGraw-Hill, New York, 1972.

[39] A. Tesei and C. S. Regazzoni, *HOS-based generalized noise PDF models for signal detection optimization*, Signal Processing **65** (1998), 267–281.

[40] C. Tison, J.-M. Nicolas, and F. Tupin, *Accuracy of Fisher distributions and log-moment estimation to describe histograms of high-resolution SAR images over urban areas*, Proceedings of the IGARSS Conference, July 21-25, Toulouse (France), 2003.

[41] H. L. Van Trees, *Detection, estimation and modulation theory*, vol. 1, John Wiley & Sons., New York, 1968.

[42] V. N. Vapnik, *Statistical learning theory*, John Wiley and Sons Inc., 1998.

[43] J. Weston, A. Gammerman, M. Stitson, V. Vapnik, V. Vovk, and C. Watkins, *Support vector density estimation*, pp. 293–306, in "Advances in Kernel Methods Support Vector Learning", B. Schölkopf, C. J. C. Burges, and A. J. Smola editors, MIT Press, Cambridge, MA, U.S.A., 1999.

[44] S. H. Yueh and J. A. Kong, *K distribution and polarimetric terrain radar clutter*, J. Electromagn. Waves Applicat. **3** (1999), no. 8, 747–768.



Unité de recherche INRIA Sophia Antipolis
2004, route des Lucioles - BP 93 - 06902 Sophia Antipolis Cedex (France)

Unité de recherche INRIA Lorraine : LORIA, Technopôle de Nancy-Brabois - Campus scientifique
615, rue du Jardin Botanique - BP 101 - 54602 Villers-lès-Nancy Cedex (France)
Unité de recherche INRIA Rennes : IRISA, Campus universitaire de Beaulieu - 35042 Rennes Cedex (France)
Unité de recherche INRIA Rhône-Alpes : 655, avenue de l'Europe - 38330 Montbonnot-St-Martin (France)
Unité de recherche INRIA Rocquencourt : Domaine de Voluceau - Rocquencourt - BP 105 - 78153 Le Chesnay Cedex (France)

Éditeur
INRIA - Domaine de Voluceau - Rocquencourt, BP 105 - 78153 Le Chesnay Cedex (France)
http://www.inria.fr
ISSN 0249-6399